

OPEN ACCESS

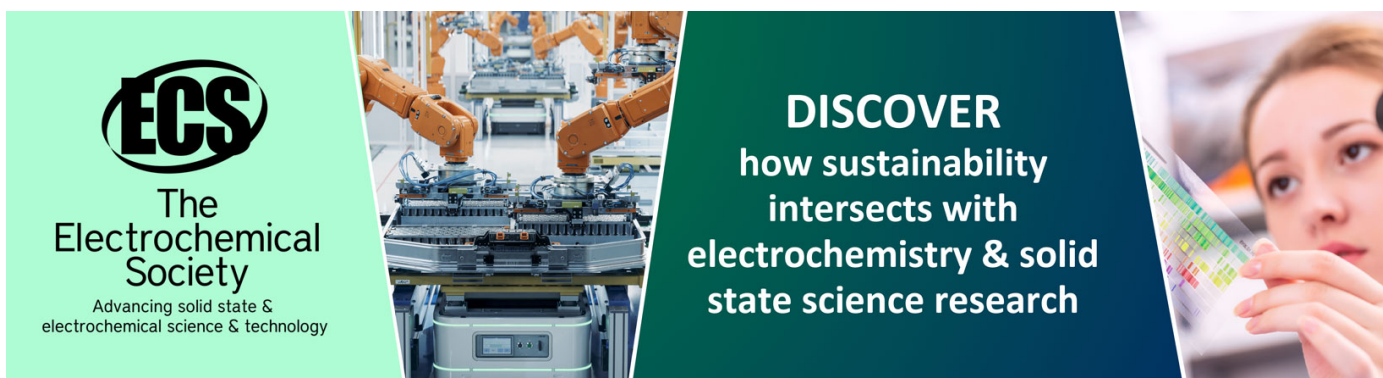
Radiation background with the CMS RPCs at the LHC

To cite this article: S. Costantini *et al* 2015 *JINST* **10** C05031

View the [article online](#) for updates and enhancements.

You may also like

- [Gamma ray background radiation for glass electrode RPCs in the CMS/LHC environment. estimation approach with GEANT4 Monte Carlo simulation packages](#)
J T Rhee, Christopher Chun, M Jamil et al.
- [Effects of the vortex line shape on the critical current density in high \$T_c\$ superconducting film with nanorod pinning centers](#)
Y Jung, K Kwak, W Lee et al.
- [Boltzmann equation and Monte Carlo studies of electron transport in resistive plate chambers](#)
D Bošnjakovi, Z Lj Petrovi, R D White et al.



ECS
The Electrochemical Society
Advancing solid state & electrochemical science & technology

DISCOVER
how sustainability intersects with electrochemistry & solid state science research

12th WORKSHOP ON RESISTIVE PLATE CHAMBERS AND RELATED DETECTORS,
23–28 FEBRUARY 2014,
TSINGHUA UNIVERSITY, BEIJING, CHINA

Radiation background with the CMS RPCs at the LHC

S. Costantini,^{f,1} Y. Ban,^a J. Cai,^a Q. Li,^a S. Liu,^a S. Qian,^a D. Wang,^a Z. Xu,^a
F. Zhang,^a Y. Choi,^b J. Goh,^b D. Kim,^b S. Choi,^c B. Hong,^c J.W. Kang,^c M. Kang,^c
J.H. Kwon,^c K.S. Lee,^c S.K. Lee,^c S.K. Park,^c L.M. Pant,^d A.K. Mohanty,^d
R. Chudasama,^d J.B. Singh,^e V. Bhatnagar,^e A. Mehta,^e R. Kumar,^e
S. Cauwenbergh,^f A. Cimmino,^f S. Crucy,^f A. Fagot,^f G. Garcia,^f A. Ocampo,^f
D. Poyraz,^f S. Salva,^f F. Thyssen,^f M. Tytgat,^f N. Zaganidis,^f W.V. Doninck,^g
A. Cabrera,^h L. Chaparro,^h J.P. Gomez,^h B. Gomez,^h J.C. Sanabria,^h C. Avila,^h
A. Ahmad,ⁱ S. Muhammad,ⁱ M. Shoaib,ⁱ H. Hoorani,ⁱ I. Awan,ⁱ I. Ali,ⁱ W. Ahmed,ⁱ
M.I. Asghar,ⁱ H. Shahzad,ⁱ A. Sayed,^j A. Ibrahim,^j S. Aly,^j Y. Assran,^j A. Radi,^j
T. Elkafrawy,^j A. Sharma,^k S. Colafranceschi,^k M. Abbrescia,^l C. Calabria,^l
A. Colaleo,^l G. Iaselli,^l F. Loddo,^l M. Maggi,^l S. Nuzzo,^l G. Pugliese,^l R. Radogna,^l
R. Venditti,^l P. Verwilligen,^l L. Benussi,^m S. Bianco,^m D. Piccolo,^m P. Paolucci,ⁿ
S. Buontempo,ⁿ N. Cavallo,ⁿ M. Merola,ⁿ F. Fabozzi,ⁿ O.M. Iorio,ⁿ A. Braghieri,^o
P. Montagna,^o C. Riccardi,^o P. Salvini,^o P. Vitulo,^o I. Vai,^o A. Magnani,^o A. Dimitrov,^p
L. Litov,^p B. Pavlov,^p P. Petkov,^p A. Aleksandrov,^q V. Genchev,^q P. Iaydjiev,^q
M. Rodozov,^q G. Sultanov,^q M. Vutova,^q S. Stoykova,^q R. Hadjiiska,^q H.S. Ibargüen,^r
M.I.P. Morales,^r S.C. Bernardino,^r I. Bagaturia,^s Z. Tsamalaidze,^s I. Crotty,^t and
M.S. Kim^u on behalf of the CMS collaboration

^aPeking University, Department of Technical Physics,
CN-100 871 Beijing, China

^bDepartment of Physics, SungKyunKwan University,
2066, Seobu-ro, Jangahn-gu, Suwon, Gyeonggi-do, Republic of Korea

^cDepartment of Physics and Korea Detector Laboratory, Korea University,
Aman-dong 5-ga, Sungbuk-gu, Seoul, Republic of Korea

^dBARC, Electronics Division (BARC),
Trombay, Mumbai 400 085, India

¹Corresponding author.

^e*Panjab University, Department of Physics,
Chandigarh Mandir 160 014, India*

^f*Ghent University, Department of Physics and Astronomy,
Proeftuinstraat 86, BE-9000 Ghent, Belgium*

^g*VUB, Dienst Elementaire Deeltjes,
Pleinlaan 2 BE-1050 Brussel*

^h*Universidad de Los Andes, Apartado Aéreo 4976,
Carrera 1E, no. 18A 10, CO-Bogotá, Colombia*

ⁱ*Islamabad-NCP, Quaid-I-Azam University,
Islamabad-44000 Pakistan*

^j*Academy of Scientific Research and Technology of the Arab Republic of Egypt,
101 Sharia Kasr El-Ain, Cairo, Egypt*

^k*CERN,
CH-1211 Geneva 23, Switzerland*

^l*Università e INFN, Sezione di Bari,
Via Orabona 4, IT-70126 Bari, Italy*

^m*INFN, Laboratori Nazionali di Frascati,
PO Box 13, Via Enrico Fermi 40, IT-00044 Frascati, Italy*

ⁿ*Università e INFN, Sezione di Napoli, Complesso Univ. Monte S. Angelo,
Via Cintia, IT-80126 Napoli, Italy*

^o*Università e INFN, Sezione di Pavia,
Via Bassi 6, IT-Pavia, Italy*

^p*University of Sofia, Faculty of Physics, Atomic Physics Department,
5, James Bourchier Boulevard, BG-1164 Sofia, Bulgaria*

^q*Bulgarian Academy of Sciences, Inst. for Nucl. Res. and Nucl. Energy,
Tzarigradsko shaussee Boulevard 72, BG-1784 Sofia, Bulgaria*

^r*Benemérita Universidad Autónoma de Puebla,
Av. San Claudio y 18 sur, edif. 111 A Ciudad Universitaria,
Col. San Manuel, Puebla, Pue. C.P. 72570, Mexico*

^s*Tbilisi-IHEPI, Tbilisi State University,
University Street 9 GE-380 086 Tbilisi*

^t*University of Wisconsin, Department of Physics 1150,
University Avenue Madison, WI 53706 U.S.A.*

^u*Kyungpook National University, Department of Physics,
80 Daehakro, Bukgu, Daegu, 702-701, Republic of Korea*

E-mail: silvia.costantini@cern.ch

ABSTRACT: The Resistive Plate Chambers (RPCs) are employed in the CMS Experiment at the LHC as dedicated trigger system both in the barrel and in the endcap. This article presents results of the radiation background measurements performed with the 2011 and 2012 proton-proton collision data collected by CMS. Emphasis is given to the measurements of the background distribution inside the RPCs. The expected background rates during the future running of the LHC are estimated both from extrapolated measurements and from simulation.

KEYWORDS: Performance of High Energy Physics Detectors; Resistive-plate chambers

ARXIV EPRINT: [1406.2859](https://arxiv.org/abs/1406.2859)

Contents

1	Introduction	1
2	The CMS RPCs at the LHC	2
3	Background measurement technique	3
4	Background measurement results	4
4.1	Linear dependence on instantaneous luminosity	4
4.2	Background as a function of z and plus-minus asymmetry	4
4.3	Background as a function of R	5
4.4	Background as a function of ϕ and azimuthal asymmetry	6
4.5	Background distribution: summary maps	7
4.6	Comparison with the CMS CSCs and DTs	8
5	Extrapolation to higher luminosities	8
6	Comparison with simulation	8
7	Conclusions	9

1 Introduction

Three years (2010-2012) of proton-proton (pp) running at the Large Hadron Collider (LHC) have provided the opportunity to extensively study the radiation background and therefore to obtain a very detailed knowledge of the background distribution in the Muon system of the Compact Muon Solenoid (CMS) [1, 2] detector. The measurements presented in this note have been performed with 2011 and 2012 runs of pp collisions at a center-of-mass energy of 7 TeV and at 8 TeV, respectively. The maximum instantaneous luminosity reached $7.7 \cdot 10^{33} \text{ cm}^{-2} \text{ s}^{-1}$ in 2012. Previous results with CMS 2010 data at 7 TeV are reported in [3].

Background studies play a decisive role with respect to the performance of the existing detector, as well as to the design of the upgraded Muon system for the High Luminosity running of the LHC (HL-LHC). In general, background radiation levels are an important consideration in the overall performance of the Muon system, and are carefully monitored. Any background source, including low energy neutrons or photons, electrons and positrons, punch-through hadrons, low momentum primary and secondary muons, and beam-induced background (particles produced in the interaction of the beams with collimators, residual gas, and beam pipe components), could affect the muon trigger performance and pattern recognition of muon tracks. In particular, spurious hits due to noise or to radiation background could promote low transverse-momentum muons to

higher momentum. In addition, excessive radiation levels could cause aging of the detectors. Furthermore, the expected radiation levels during the HL-LHC can contribute to drive the choice of the most suitable technology for the detector upgrade. Reliable estimates of the expected hit rates are therefore essential.

2 The CMS RPCs at the LHC

CMS is one of the six experiments currently operating at the LHC. The central feature of the general-purpose CMS detector is a superconducting solenoid, of 6 m internal diameter, providing a magnetic field of 3.8 T. Muons with pseudorapidity in the range $|\eta| < 2.4$ are measured in gas-ionization detectors embedded in the steel return yoke, with detection planes made of three technologies: Drift Tube (DT) chambers, Cathode Strip Chambers (CSC) and Resistive Plate Chambers (RPC).

The RPC [3–5] detectors are implemented in CMS as a dedicated trigger system, in both the barrel and the endcap regions. Figure 1 shows a schematic view of one quarter of the CMS detector in the R-z plane and figure 2 the layout of a double-gap barrel chamber. Two gas gaps, of 2 mm each, are formed by two parallel phenolic-melaminic laminate (bakelite) electrodes, with one single plane of copper readout strips in-between. The two gaps feature 2 mm thickness and have a bulk resistivity of the order of $10^{10}\Omega$ cm. High Voltage (HV) is applied to the outer graphite-coated surface of the bakelite plates. The chambers are equipped with front-end boards. The CMS RPCs work in saturated avalanche mode and use a three-component, non-flammable gas mixture composed of 95.2% $C_2H_2F_4$ (R134a), 4.5% iC_4H_{10} (isobutane) and 0.3% SF_6 . After mixing, water vapor is added in order to maintain the relative humidity at constant values of 40%-50% and to allow for constant bakelite resistivity.

The barrel RPC system consists of five wheels, installed at $|\eta| < 0.8$ and $|z| < 7$ m, subdivided into 12 azimuthal sectors, each one equipped with six radial layers of RPCs. The radial layers are referred to in the following as RB1, RB2, RB3 and RB4 (two RB1 and two RB2 layers exist, for a total of six radial layers). Six endcap disks, three on the positive and three on the negative endcap side, are divided into 36 azimuthal sectors, with two radial rings (labeled R2 and R3) in each one. They assure a full coverage up to $|\eta| < 1.6$, as shown in figure 1. The fourth endcap disks, one on each side, are being installed during the 2014 shutdown and were not present during the 2010-2012 data taking period. The innermost rings (R1) will be installed during a future shutdown.

In total, 480 barrel chambers and 432 endcap chambers were installed and operated in the 2010-2012 data taking period, adding up to 68136 barrel strips and 41472 endcap strips, respectively, and covering a total surface of about 3000 m². The strip pitch dimensions are between 2.28 and 4.10 cm in the barrel and between 1.95 and 3.63 cm in the endcap.

The RPCs have performed very well, with more than 98% of the channels operational. They were responsible for less than 1% of the CMS running time loss, mainly due to a single episode of failure of a power supply. The fraction of recorded pp collision data certified good by the RPCs was above 99% in 2010–2012.

In 2011 (2012) CMS has recorded 5.2 (21.8) fb⁻¹ of data out of 5.7 (23.3) fb⁻¹ delivered by the LHC, for an efficiency of 91 (about 94) %. Roughly 93% of the recorded data have been certified as “golden” for all physics analyses. Only certified runs have been used for the background studies.

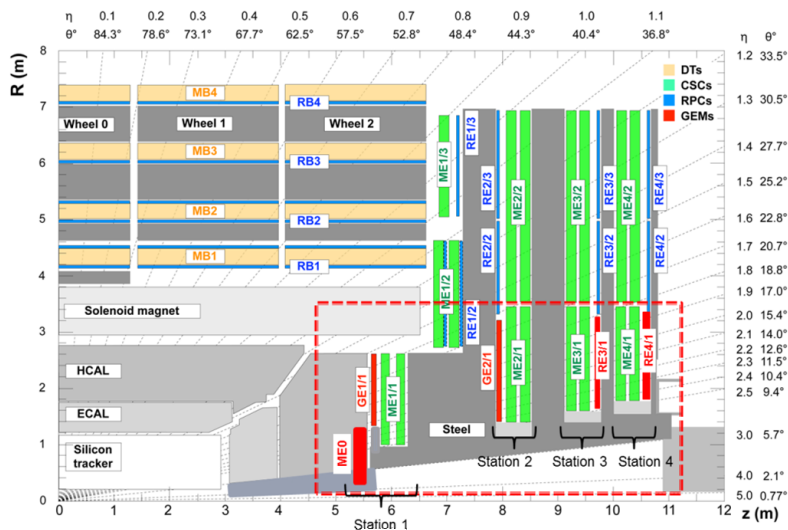


Figure 1. Schematic view, in the R-z plane, of one quadrant of the CMS detector, with the axis parallel to the beam (z) running horizontally and the radius (R) increasing upward. The interaction region is at the lower left corner. The position of the present RPC chambers is shown in blue. The RPCs are both in the barrel (“RB” chambers) and in the endcaps (“RE”) of CMS. The DT chambers are labeled “MB” (“muon barrel”) and the CSC chambers are labeled “ME” (“muon endcap”). The steel disks are displayed as dark gray areas. Also shown in red are the chambers of the proposed upgrade scenario of the CMS Muon system, including Gas Electron Multiplier detectors (labeled “ME0” and “GE”) and RPCs (“RE3/1” and “RE4/1”).

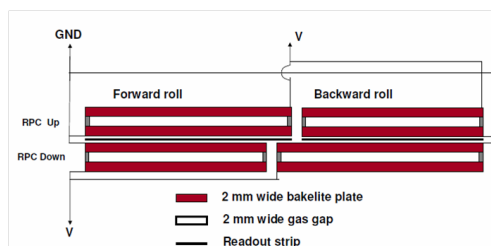


Figure 2. Schematic layout of a double-gap barrel chamber composed by two sub-units, called rolls. The readout strip plane is also shown.

3 Background measurement technique

The RPC hit rate is measured at the strip level during LHC pp collision runs. The strip rate is calculated by using the incremental counts of the RPC trigger Link Boards. The incremental counts are taken during typical time intervals of the order of 100 s. The resulting rates are then averaged over the total runtime and normalized to the strip area. The instantaneous luminosity is averaged over the same runtime. Normalized rates in Hz/cm² are shown in this paper.

No trigger selection is applied at this stage, resulting in an inclusive measurement of the radiation background rates. The offset level due to the intrinsic noise is estimated (if present) for each run and each chamber separately through a linear extrapolation to the value corresponding to zero instantaneous luminosity, which is subtracted from the chamber rate. The average noise rate measured during 2010-2012 cosmic runs is of the order of 0.1 Hz/cm², as shown in figure 3 (left), i.e. much lower than the average background rates shown in section 4.

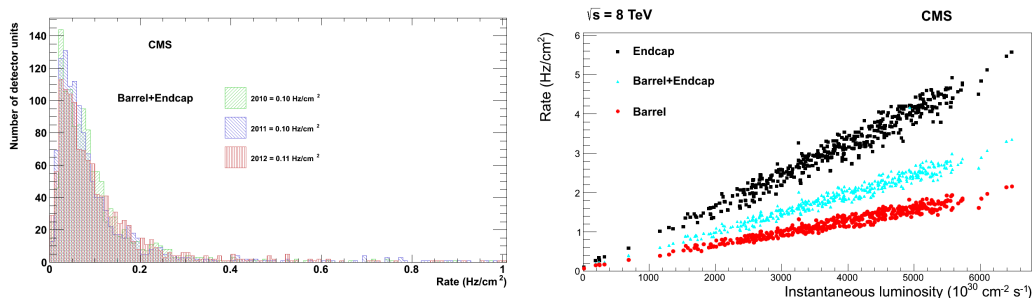


Figure 3. Left: average noise rate measured in the whole RPC detector, in 2010 (light green), 2011 (blue), and 2012 (dark red) in absence of pp collisions, during cosmic runs. The average noise level is approximately 0.1 Hz/cm^2 , constant in time. Right: average background rate as a function of the instantaneous luminosity, measured in 2012 in the RPC barrel (red) endcap (black) and in the total system (barrel plus endcap, shown in light blue).

4 Background measurement results

4.1 Linear dependence on instantaneous luminosity

A linear relationship has been observed between the measured RPC hit rate and the LHC instantaneous luminosity, for several orders of magnitude from $10^{29} \text{ cm}^{-2} \text{ s}^{-1}$ in 2010 to almost $10^{34} \text{ cm}^{-2} \text{ s}^{-1}$ in 2012. The linear relationship holds not only for every single chamber, with correlation coefficients greater than 80% in roughly 95% of the chambers (and specifically greater than 95% in more than 80% of the chambers) and also for larger detector parts (layers, rings, disks, wheels, etc.), as displayed in the following figures showing the measured rate as a function of the luminosity.

No deviation from linearity has been observed in the 2010–2012 range of the LHC luminosity, therefore excluding, in this range, phenomena which could give rise to power-law dependence relationships with exponent different from 1. Extrapolations from the present measurements to larger luminosity values have thus been performed linearly and are reported in section 5. Figure 3 (right) shows the average background rates measured in the RPC detector as a function of the instantaneous luminosity. Larger average rates are measured in the endcap, which spans a higher $|\eta|$ region.

4.2 Background as a function of z and plus-minus asymmetry

In the central $|\eta| < 0.8$ region the rates increase along z as the chambers are further from the interaction point (IP), with the largest rates observed in the outermost wheels $W + 2$ and $W - 2$ (figure 4), which are the ones most exposed to the slow neutron gas permeating the cavern. The asymmetry between the two external wheels, with larger rate measured on the positive side ($W + 2$) with respect to the negative side ($W - 2$), might be due to lower density of the neutron gas on the negative side because of the presence of the CMS main shaft (through which the detector was lowered from the surface into the cavern).

The same pattern is observed at high $|\eta|$ (in the endcap, figure 5), with higher rate as $|\eta|$ increases, *i.e.* in the chambers located further away from the IP. Both the inner (R2) and the outer (R3) rings of the six endcap disks show an increasing background as z increases.

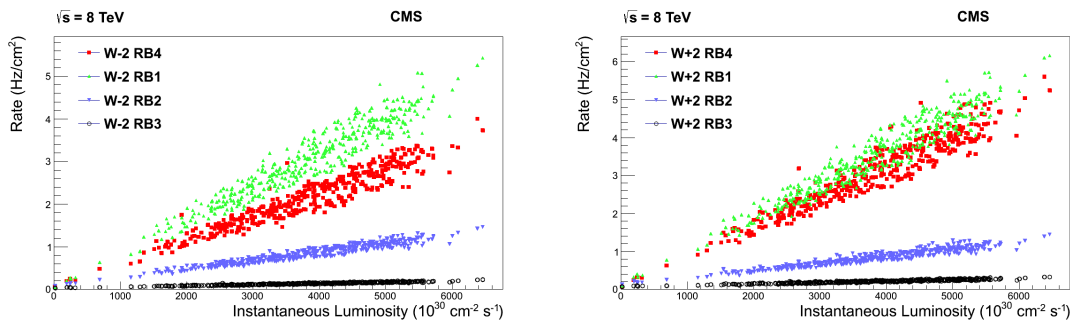


Figure 4. Background rate in the radial layers of W-2 (left) and W+2 (right). Larger rates are measured in the innermost (RB1) and outermost (RB4) layers, as discussed in the text. The plus-minus asymmetry of the RB4 layers of the external wheels can also be appreciated from the comparison between the two plots, showing higher background levels on the plus side.

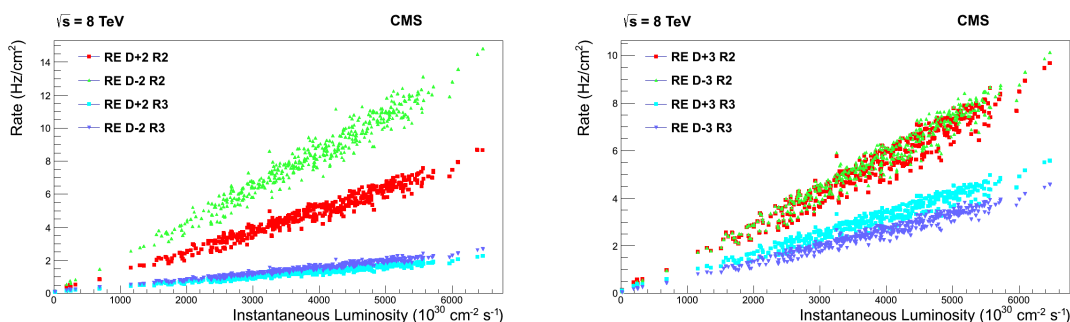


Figure 5. Background rate in the disks D-2 and D+2 (left) and D-3 and D+3 (right). For each disk, the two radial rings R2 and R3 are shown.

It is interesting to note (figure 5, left) the asymmetry between the rings R2 of the negative (labeled “D-2 R2”) and the positive (labeled “D+2 R2”) second disk of the endcap, due to missing shielding tiles on the negative endcap yoke supporting the disk D-2.

4.3 Background as a function of R

The background behavior as a function of R is different in the barrel and in the endcap, reflecting the different types of background sources near the beamline and on the outside of CMS.

In the barrel (figure 4), the largest background is observed both in the inner layers (RB1), and in the outer layers (RB4). The innermost chambers are exposed to particle leakage from the hadron calorimeter, and from the gap between the barrel and the endcap of the calorimeters, while the barrel outermost chambers are mostly exposed to the surrounding radiation background from slow neutrons. Chambers located in the central layers RB2 and RB3 are protected by the steel of the barrel wheels and therefore detect much lower rates.

In the endcap (figure 5), the highest rates are detected in the inner rings (rings R2 of all endcap disks). The radial rings R2 are the closest to the beamline. The background rates decrease along R as the distance from the beamline increases. The outer (R3) chambers show a smaller increase in rate with luminosity relative to the inner (R2) chambers.

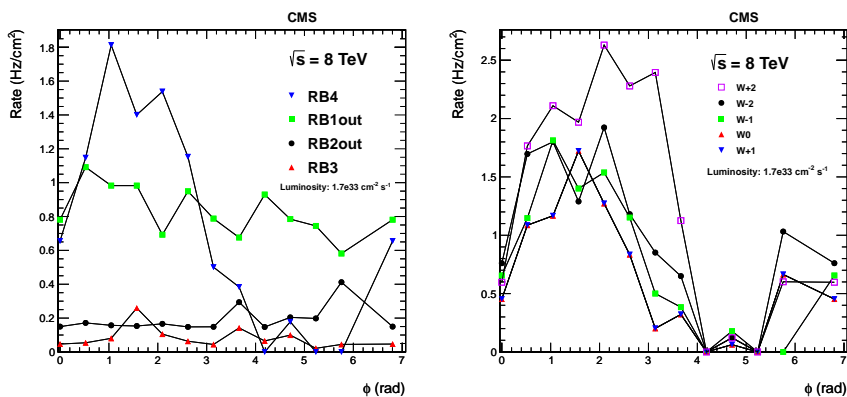


Figure 6. Left: Background rates of RPC chambers located in inner and outer layers of the barrel wheel W-1, as a function of the chamber azimuthal position, for a luminosity of $1.7 \cdot 10^{33} \text{ cm}^{-2} \text{ s}^{-1}$ in 2012. A dependence on the chamber azimuthal position (ϕ asymmetry) is shown for the external layer RB4. Right: Background rates of the RB4 layers in all barrel wheels. The larger rate in the W+2 wheel is discussed in the text.

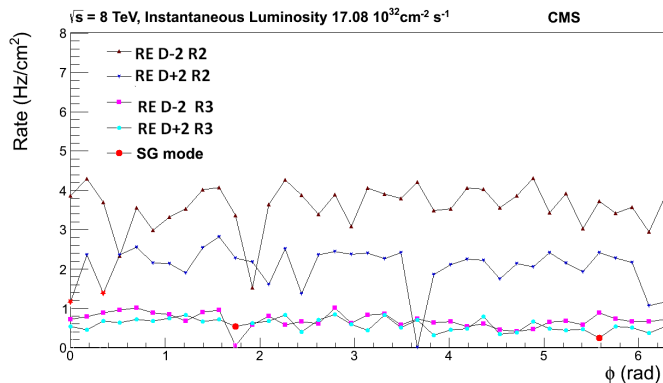


Figure 7. Background rates of RPC chambers located in the rings R2 and R3 of the endcap disks D+2 and D-2, as a function of the chamber azimuthal position, for a luminosity of $1.7 \cdot 10^{33} \text{ cm}^{-2} \text{ s}^{-1}$ in 2012. Note the higher rate in D-2/R2, mentioned in the text.

4.4 Background as a function of ϕ and azimuthal asymmetry

A strong azimuthal dependence of the background has been observed in the outer barrel layers (RB4) of all barrel wheels (figure 6), while in the inner layers the background distribution is symmetrical. In RB4 the rate ratio between the top and the bottom sectors is approximately a factor 20. The top-bottom asymmetry is explained by the non-symmetric features of the -otherwise symmetric- CMS detector: the concrete and steel flooring and the wheel and disk supports.

No evidence of ϕ -asymmetry is observed in the endcap (figure 6), most likely because the endcap chambers are located in between steel disks, while the barrel outer top chambers (RB4, top ϕ sectors from 3 to 5) are more exposed to the surrounding background.

4.5 Background distribution: summary maps

The background measurement results described in details in the previous sections are also visually summarized in the two-dimensional plots shown in figures 8 and 9. In the barrel, larger rates are measured in the top (3,4,5) sectors of RB4, and in the internal radial layer RB1, independently of the sector. In the endcap, the rates are higher close to the beamline. The maps show no evidence of ϕ asymmetry in the endcap.

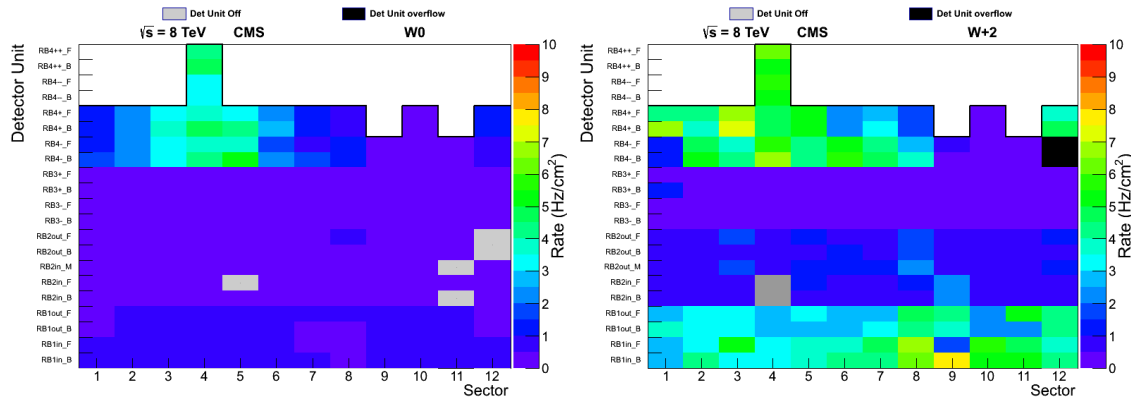


Figure 8. Two-dimensional maps of the background distribution in the central barrel Wheel 0 (left), and in the external positive Wheel+2, where the highest rate is detected. Each box represents a detector unit in the $R - \phi$ plane. The chambers are ordered from RB1 to RB4, for increasing radial distance from the beamline, and along the azimuthal trigger sectors. “Det Unit Off” indicates chambers switched off, while “Det Unit overflow” represents single noisy chambers not used in this analysis.

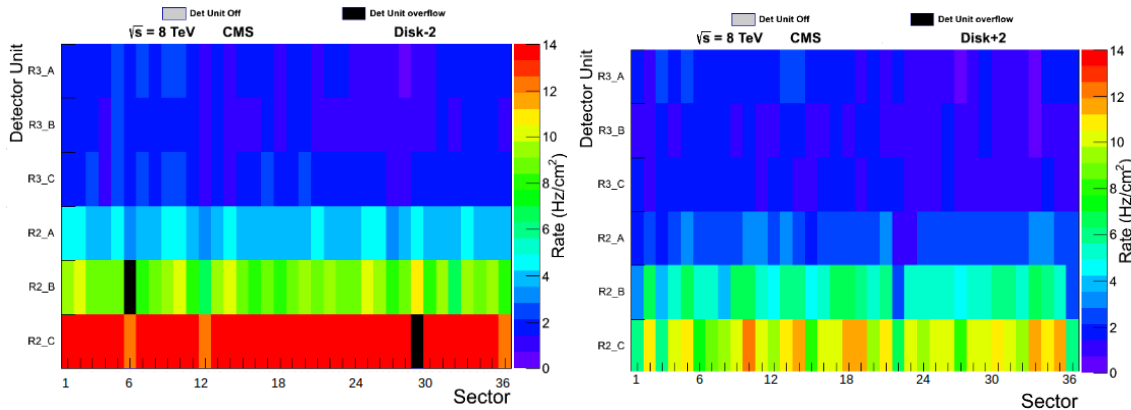


Figure 9. Two-dimensional maps of the background distribution in the endcap Disk-2, where the highest rate is detected (as explained in the text), and in the Disk+2. Each box represents a detector unit in the $R - \phi$ plane. The chambers are ordered radially in η partitions with increasing radial distance from the beamline (with partition C of ring R2 being the closest to the beamline), and along the azimuthal trigger sectors. “Det Unit Off” indicates chambers switched off, while “Det Unit overflow” represents single noisy chambers not used in this analysis.

4.6 Comparison with the CMS CSCs and DTs

Similar features of the radiation background distributions as a function of R , z , and ϕ , have been measured also by the CSCs and DTs, including the linear dependence on the LHC instantaneous luminosity. A comparison with 2010 data among the three detectors of the CMS Muon system was performed in [3].

5 Extrapolation to higher luminosities

Based on the linear relationship between measured rates and instantaneous luminosity, the RPC rates can be linearly extrapolated to higher luminosity values.

The extrapolation to higher beam energy (from 7 or 8 TeV of the present pp data to 14 TeV) can be performed by rescaling by an approximate total factor of 1.5, due to larger cross section and particle multiplicity: the pp inelastic cross section increases from 73.5 mb [6] at 7 TeV to 80 mb [7] at 14 TeV; a factor $\sqrt{2}$ accounts for the increased particle multiplicity, scaling as square root of the energy.

At a peak luminosity of 10^{34} (or $5 \cdot 10^{34}$) $\text{cm}^{-2} \text{s}^{-1}$, and at the center-of-mass energy of 14 TeV, the expected average rates are of the order of 4 (20) Hz/cm^2 in the barrel and 12 (60) Hz/cm^2 in the endcap. The maximum rates in the most exposed regions of the RPCs are within a factor 5 with respect to the quoted average rates, and are therefore well within the RPC rate capability, which is of the order of 1 kHz/cm^2 [8].

6 Comparison with simulation

Comparisons with FLUKA [9] simulated data have shown that the simulation describes well the typical patterns of the radiation background inside the RPCs. Figure 10 (left) shows, as an example, the neutron flux inside the Muon system. As measured in the data, the flux is expected to be higher in the RB1 and RB4 barrel layers, and in the endcap at high $|\eta|$, with respect to other detector parts. The reference luminosity of $10^{34} \text{cm}^{-2} \text{s}^{-1}$ is assumed.

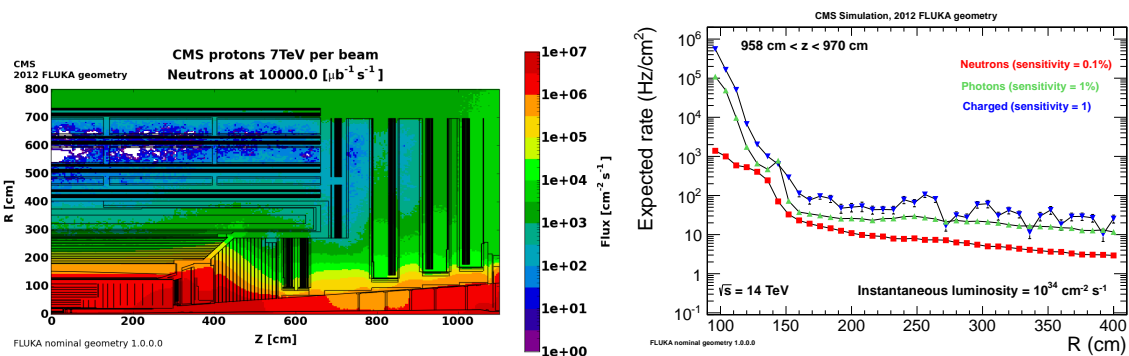


Figure 10. Left: Expected neutron flux, in Hz/cm^2 , in the Muon system. An R - z view of one quarter of the CMS detector is shown. Right: Expected rate, from neutrons, photons, and charged particles, as a function of the radial distance from the beamline, for a z distance between 790 and 802 cm from the IP. The future RE3/1 ring will cover the radial range between 160 and 330 cm.

Flux and rate estimates from simulation can be used in the high $|\eta|$ regions -not covered by the present Muon system- where additional RPC chambers will be installed in a future shutdown. In order to provide estimates of the expected rates, the FLUKA flux values have been rescaled by the following average sensitivity values [10] from previous simulations and test beam measurements: 0.001 for neutrons, 0.01 for photons, and 1 for charged particles. Neutrons, photons, and charged particles account for almost 100% of the particles produced in primary pp interactions. In total, a rate of a few tens of Hz/cm² is expected at low R and high $|\eta|$ values, i.e. in the region closest to the beamline (figure 10, right).

7 Conclusions

Detailed studies of the radiation background have been performed, which have led to an accurate understanding of the background distribution inside the CMS Muon system. Comparisons with simulations have shown reasonable agreement between the measurements and the expected rates. Extrapolations to high-luminosity scenarios predict background levels within the RPC rate capability.

Acknowledgments

Acknowledgments of support of all CMS are given in ref. [3]. The authors would like to thank the RPC2014 organizers and the colleagues of the CMS Muon system.

References

- [1] CMS collaboration, *The Compact Muon Solenoid*, Technical Proposal, CERN-LHCC-094 (1994).
- [2] CMS collaboration, *The CMS Experiment at the CERN LHC*, 2008 *JINST* **3** S08004.
- [3] CMS collaboration, *The performance of the CMS muon detector in proton-proton collisions at $\sqrt{s} = 7$ TeV at the LHC*, 2013 *JINST* **8** P11002.
- [4] M. Abbrescia et al., *Cosmic ray tests of double-gap resistive plate chambers for the CMS experiment*, *Nucl. Instrum. Meth. A* **550** (2005) 116.
- [5] CMS collaboration, *Performance Study of the CMS Barrel Resistive Plate Chambers with Cosmic Rays*, 2010 *JINST* **5** T03017 and references therein.
- [6] TOTEM collaboration, *First measurement of the total proton-proton cross section at the LHC energy of $\sqrt{s} = 7$ TeV*, *Eur. Phys. Lett.* **96** (2011) 21002.
- [7] T. Pierog, I. Karpenko, J.M. Katzy, E. Yatsenko and K. Werner, *EPOS LHC: test of collective hadronization with LHC data*, [arXiv:1306.0121](https://arxiv.org/abs/1306.0121).
- [8] M. Abbrescia, *The dynamic behaviour of Resistive Plate Chambers*, *Nucl. Instrum. Meth. A* **533** (2004) 7.
- [9] Fluka team, www.fluka.org; Matplotlib team, www.matplotlib.org; citations and credits therein.
- [10] S. Altieri et al., *RPC gamma sensitivity simulation*, *Nucl. Instrum. Meth. A* **456** (2000) 99; *Simulation of Resistive Plate Chamber sensitivity to neutrons*, *Nucl. Instrum. Meth. A* **461** (2001) 57.